NANO LETTERS

Letter

pubs.acs.org/NanoLett

Lateral and Temporal Dependence of the Transport through an Atomic Gold Contact under Light Irradiation: Signature of Propagating Surface Plasmon Polaritons

Daniel Benner, Johannes Boneberg, Philipp Nürnberger, Reimar Waitz, Paul Leiderer, and Elke Scheer*

Department of Physics, University of Konstanz, Universitätsstraße 10, 78464 Konstanz, Germany

Supporting Information

ABSTRACT: Metallic point contacts (MPCs) with dimensions comparable to the Fermi wavelength of conduction electrons act as electronic waveguides and might operate as plasmon transmitters. Here we present a correlated study of optical and conductance response of MPCs under irradiation with laser light. For elucidating the role of surface plasmon polaritons (SPPs), we integrate line gratings into the leads that increase the SPP excitation efficiency. By analyzing spatial, polarization, and time dependence, we identify two SPP contributions that we attribute to transmitted and decaying SPPs, respectively. The results demonstrate the role of SPPs for optically controlling the transport in metallic nanostructures and are important for designing opto-nanoelectronic devices.

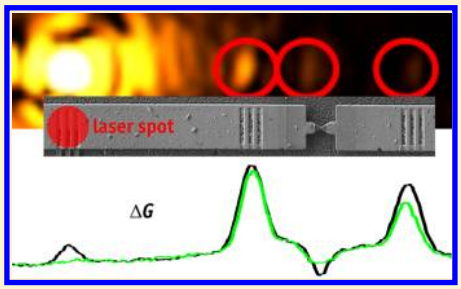

KEYWORDS: *Surface plasmon polariton (SPP), photo-assisted transport (PAT), atomic contact, field enhancement, polarization dependence, optical antennae*

Metallic contacts with the lateral size of one atom have shown to be ideal testbeds for probing novel low-dimensional and quantum transport phenomena. Metallic point contacts (MPCs) accommodate a small number of quantum mechanical transport channels[1,2] resulting in a conductance in the order of the conductance quantum $G_0 = 2e^2/h$ with the elementary charge e and Planck's constant h. Simultaneously they represent the ultimate limit of miniaturization of an electronic circuit, and much effort has been taken to explore and actively control their electronic transport properties and to elucidate potential functionalities. It has been reported before that the conductance of MPCs can be strongly influenced by irradiation with electromagnetic fields in the visible and near-infrared range.[3−7] The origin of the observed conductance change is interpreted as photoassisted transport (PAT) caused by the energy dependence of the quantum mechanical transmission function.[8]

The typical geometry of the MPCs—a fine constriction between two tapered leads with atomically fine tips—is close to the one of bow-tie optical antennae, which are known to give rise to pronounced enhancement of the local electromagnetic field at the tips.[9−15] The observed strong conductance changes may thus have been influenced by local field enhancement as well. Furthermore, it has been suggested that the excitation of surface plasmon polaritons (SPPs) may additionally contribute to the conductance changes.[3−7] The field enhancement of optical antennae can be probed by the observation of outcoupled light from an area close to the tips.[16] These investigations have been performed mainly independent of transport measurements, and only recently a correlation between conductance and optical response of metallic tunnel contacts has been reported,[15,17,18] however not in the size regime of single-atom contacts, where pronounced sample-to-sample variations are imminent,[3,4] because the transport properties depend on the exact atomic arrangement.[1,2] Here, we present the first comprehensive analysis of the correlation between SPP transmission and electronic transport through a given single-atom or few-atom contact. We study the contribution of SPPs to the conductance changes by incorporating line gratings into the leads bridging between the macroscopic electrodes and the constriction forming the MPC. A detailed analysis of the optical response of the MPC has been reported separately.[19] Since light illumination always goes along with dissipation, special care has to be given to the disentanglement of thermal and electronic effects.[3−7,20] In addition to the experiments we therefore perform time-resolved finite element (FE) simulations elucidating the behavior of a MPC specimen upon light irradiation to clearly discern between the contribution of SPPs and of dissipated heat becoming noticeable in thermal expansion to the conductance change.

We use the mechanically controllable break junction (MCBJ) technique to fabricate MPCs of gold at ambient conditions.[3,4,19] By electron beam lithography we pattern a suspended Au constriction on top of a flexible stainless steel substrate that was before covered with an electrically insulating layer of polyimide. The thickness of the gold layer is 100 nm and the length of the constriction is about 2.5 μm. Excitation gratings for the SPPs are fabricated by focused ion beam (FIB) milling. A typical

Received: June 10, 2014
Revised: July 31, 2014

   dx.doi.org/10.1021/nl502165y | *Nano Lett.* XXXX, XXX, XXX−XXX

sample carrying line gratings in the leads is shown in Figure 1. The details of the fabrication and the parameters of the gratings are given in ref 19 and in the Supporting Information (SI).

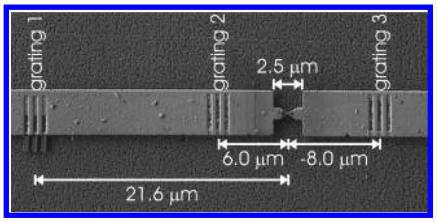

Figure 1. SEM picture of a sample showing the gratings 1, 2, and 3 on the left and the right side of the constriction; the grating period is about 760 nm with trenches of about 0.4 × 3.2 × 0.09 μm^3 in length, width, and depth. The distances d from the center of the gratings to the MPC are about 21.6 μm, 6.0 μm, and 8.0 μm (the minus sign indicates the position at the right side of the MPC).

The sample is mounted between fixed counter supports and the pushing rod of a three-point bending mechanism (see Figure S1 in the SI). By moving the pushing rod, the substrate is bent elastically, resulting in an effective length change of the constriction. The suspended part of the constriction reacts on the mechanical strain by a change of the minimal cross section, and thus a change of the electrical conductance is established. The mounted sample is multidirectionally movable by a motorized *xyz*-stage for adjusting the sample in the focal plane of a laser illumination system with an accuracy of ±250 nm.

Details of the optical microscope setup and the electronic circuit are given in the SI. We use pulses of about 2.5 μs (fwhm) with a duty cycle of 1:18 of the laser diode (wavelength 780 nm) and a repetition rate in the 10 kHz regime for inducing a conductance change. The absolute value of the light-induced conductance change ΔG is recorded by lock-in technique and by averaged time-resolved measurements (time-resolution is about 2 μs). The polarization of the electric field of the incoming light is either adjusted parallel (p-polarization) or perpendicular (s-polarization) to the transport direction. The spot diameter (fwhm) of the laser light at the surface of the sample is about 1.7 μm, and the optical resolution is about 800 nm.

In addition to the experiments we perform time-resolved heat transport simulations for the given sample geometry and materials. The simulations include the experimental details of the illumination setup as spot diameter, polarization, and laser power (for details see SI). From these simulations we extract the time-dependent displacement of the illuminated lead along the electronic transport direction toward the constriction as a function of the position of illumination.

The disentanglement of thermal and electronic effects is a challenging task in the field of electronic transport measurements under light illumination.[3−7,20] For separating these effects we excite SPPs by line gratings that are several micrometers away from the MPC, but still give rise to significant conductance changes for moderate laser irradiation and thus moderate heating of the overall sample. As shown in ref 19, for p-polarization we excite a SPP mode traveling along the air/gold interface with a decay length of roughly 12 μm. For s-polarization we found a decay length in the same range, but the measured SPP intensity at an arbitrary position along the gold stripe is at least a factor 20 smaller than for p-polarization.

Figure 2 shows the light-induced conductance change $\Delta G^{p,s}$ recorded by a lock-in technique when scanning the laser spot

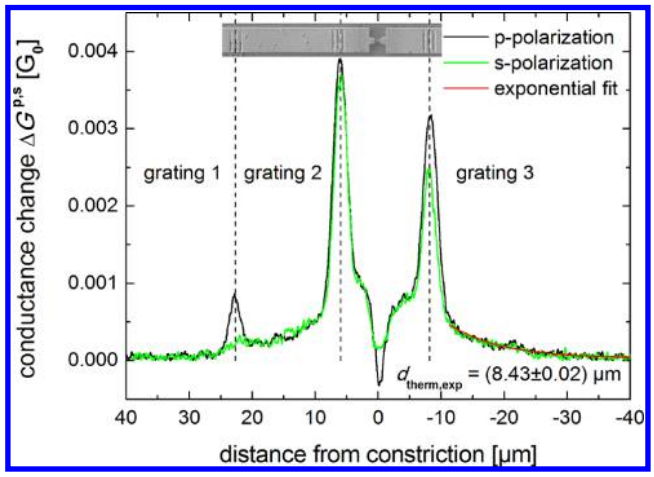

Figure 2. Light-induced conductance change $\Delta G^{p,s}$ during a scan along the long axis of the sample for p- (black) and s-polarization (green) recorded by a lock-in technique. The influence of the three gratings is clearly visible. The red line indicates a long-ranged background contribution to the conductance change caused by thermal expansion of the overall sample. The conductance G of the sample remained constant at $(1.83 \pm 0.15)\ G_0$ throughout the whole measurement.

along the long axis of the sample. The sequence of laser pulses has a time-averaged input power of 42 μW corresponding to an intensity of about 1.8 kW/cm^2. The intensity is chosen such that there is a barely detectable influence when irradiating far away from the MPC and off the gratings. The signal consists of three contributions: At first we observe a long-ranged increase of the conductance when approaching the MPC (illustrated by the red line in Figure 2). This conductance enhancement is in agreement with earlier experiments[3−7] and is discussed in the SI. The second contribution is a pronounced minimum of $\Delta G^{p,s}$ when the laser spot is located close to the MPC and is also discussed in the SI. Here, we focus on the third contribution when the laser spot is located on one of the gratings and we observe a maximum in $\Delta G^{p,s}$. The experiments are then repeated for s-polarization, where the long-ranged signal remains unchanged, but the local maxima at the gratings are reduced in amplitude, yet by a different factor: While the maxima at gratings 2 and 3 are only slightly reduced, the maximum at grating 1 is markedly suppressed, see Figure 2. This observation indicates that several contributions with a different length dependence add up to the total observed conductance changes.

Further insight is obtained from time-resolved transport measurements when irradiating at the positions of the gratings. Figure 3a and b show the relative conductance increase $dG^{p,s} = \Delta G^{p,s}/G$ versus time depending on the position of illumination for both polarizations. The power of a single laser pulse is about 432 μW corresponding to an intensity of about 18.5 kW/cm^2. For a better comparison the signals are normalized. The origin of the time axis $t = 0$ is at the maximum of the laser pulse (dashed line).

At first we observe a delay time t_{exp} between the maximum of the laser pulse and the maximum of the conductance change (for details see SI). For both polarizations t_{exp} increases with distance d. However, for p-polarization the increase is much smaller than for s-polarization, as it is most clearly visible for

dx.doi.org/10.1021/nl502165y | *Nano Lett.* XXXX, XXX, XXX−XXX

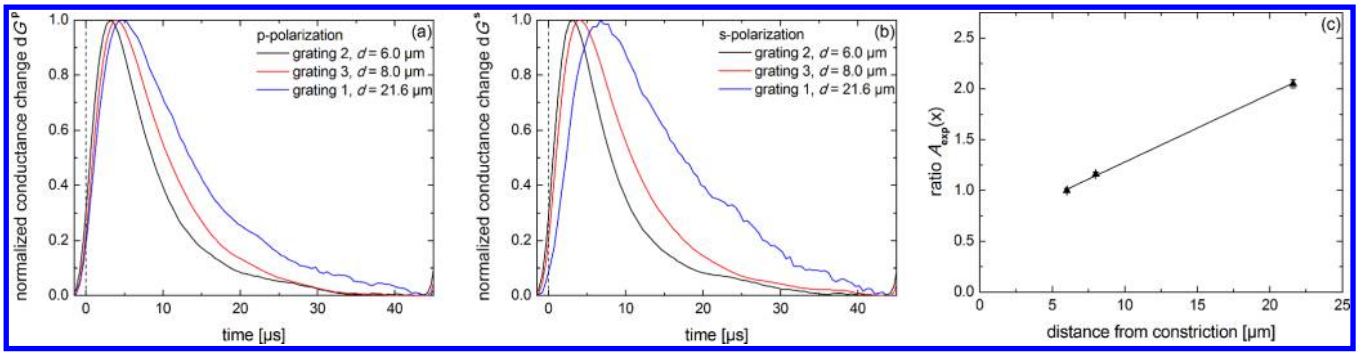

Figure 3. Time-resolved relative conductance change induced by a laser pulse depending on the position of illumination for (a) p- and (b) s-polarization. The signal amplitudes are normalized, and the time axis is set to 0 at the maximum of the laser pulse intensity. (c) Dependence of the ratio A_{exp} (see text) on the position of illumination. The ratio increases when increasing the distance d from the MPC to the illuminated gratings. The black line serves as a "guide to the eye". The error bars are smaller than the symbols. The conductance G of the sample remained constant at $(1.92 \pm 0.07)\ G_0$ throughout the whole measurement.

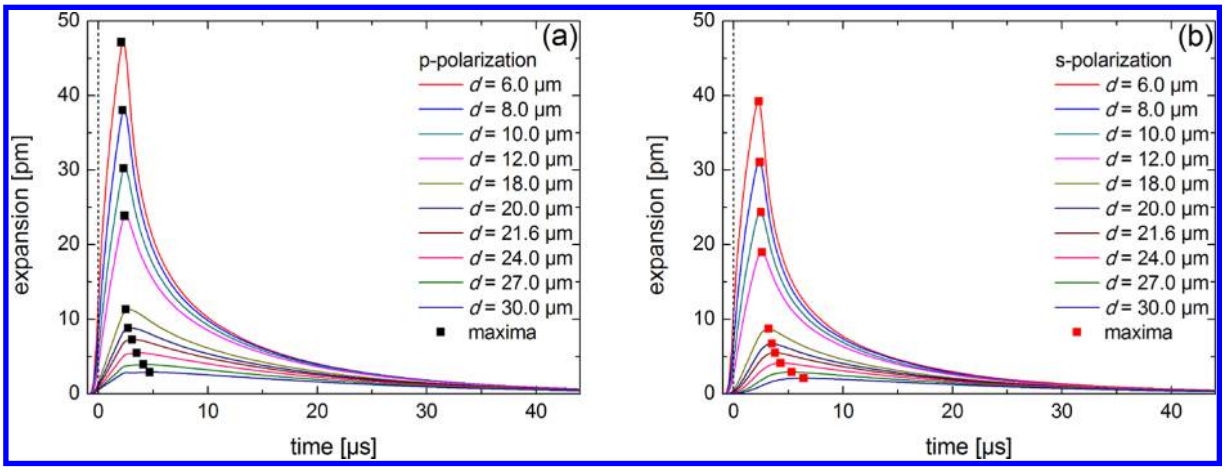

Figure 4. Calculated time-resolved thermal expansion induced by a laser/heat source depending on the position of illumination for the two polarizations ((a) p-, (b) s-polarization). By increasing the distance d from MPC to the position of illumination/heating the maxima are decreasing and appear later.

grating 1 for which the distance d between grating and MPC is largest.

For a more quantitative analysis we repeated the experiment for varying laser power. We divide the maxima of conductance changes observed in p-polarization by the maxima of conductance changes observed in s-polarization, obtaining the signal ratio $A_{exp}(x) = dG^{p}_{max}(x)/dG^{s}_{max}(x)$ individually of all gratings, where $dG^{p,s}_{max}(x) = \Delta G^{p,s}_{max}(x)/G$. Since the dG_{max} values for each polarization state depend linearly on the time-averaged input power (see Figure S9 in the SI), the ratio A_{exp} at a fixed position of illumination is independent of the power. Figure 3c shows the power-averaged values of A_{exp} depending on the position of illumination with error bars referring to this power-averaging. A_{exp} increases when increasing the distance d from the MPC to the position of illumination.

From the complex behavior of $dG^{p,s}$ and in particular the analysis of A_{exp} and t_{exp} we conclude that at least two mechanisms contribute to the total dG. The shorter delay times t_{exp} for p-polarization indicate a faster transport process from the point of illumination to the MPC than for s-polarization. We suggest the following scenario that is in agreement with our experimental findings: The SPPs excited at the gratings propagate along the stripe and give rise to heat dissipation as they decay. In simultaneously conducted experiments of the optical response, the decay length of the SPPs launched in p-polarization was shown to amount to $l = (11.7 \pm 3.3)\ \mu$m (see the SI). Since the decay length is of the same order as the distance between excitation and MPC, some fraction will arrive at the MPC and may contribute to the conductance change by photoassisted transport (PAT) as reported earlier.[3−7]

The optical response also revealed an intensity of SPPs in p-polarization that was at least a factor 20 bigger than in s-polarization. We therefore assume that in s-polarization SPPs contribute negligibly to the conductance change that is then completely caused by thermal effects. One possible thermal effect is given by enhanced light absorption at the gratings giving rise to enhanced dissipation and finally enhanced conductance by thermal expansion. However, this mechanism should give rise to a uniform ratio between the conductance changes for the two polarizations at all optical elements. Indeed, dissipation and thermal expansion depend on the initial polarization of the light, but the ratio is independent and thus a length-independent A_{exp}. The enhanced A_{exp} for long distance must be caused by a polarization-dependent and long-ranged effect, e.g., by SPPs.

For deriving additional information about thermal expansion caused on the one hand by SPP decay and on the other hand by light absorption at the gratings, we performed FE simulations (see SI-2). By the implementation of the lateral shape of the

dx.doi.org/10.1021/nl502165y | Nano Lett. XXXX, XXX, XXX−XXX

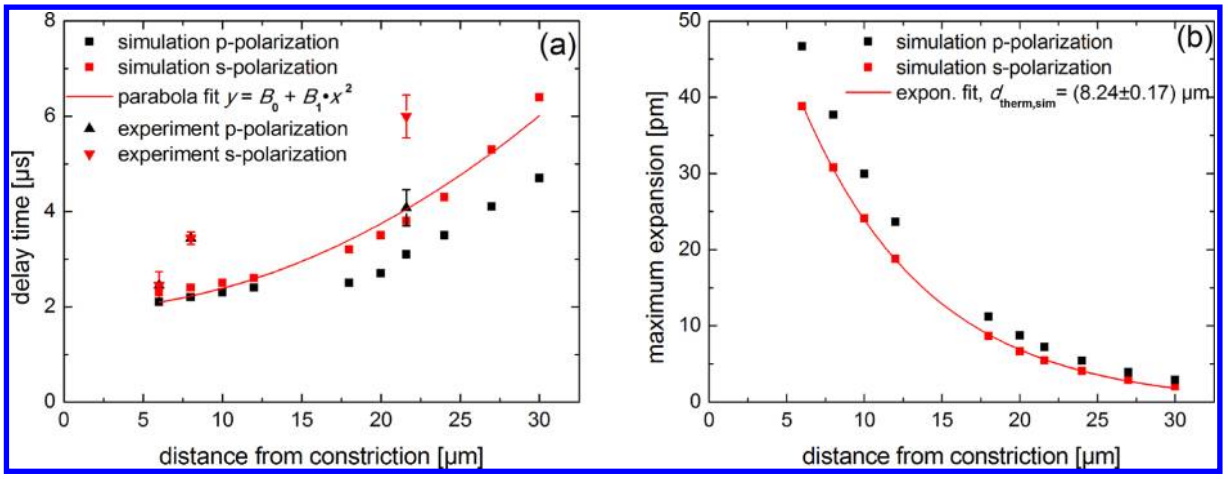

Figure 5. (a) Dependence of the delay time on the distance of illumination for the experimental (triangles) and simulation (squares) results. The delay time is increased by increasing the distance from MPC to the position of illumination. At both simulation and experiment, the delay for the perpendicular polarization (red symbols) is longer than for the parallel polarization. (b) Dependence of the calculated maxima of expansion on the distance from MPC to the position of illumination for both polarizations. Fitting the s-polarization data by an exponential decay function leads to the thermal decay length of our system of roughly 8.24 μm.

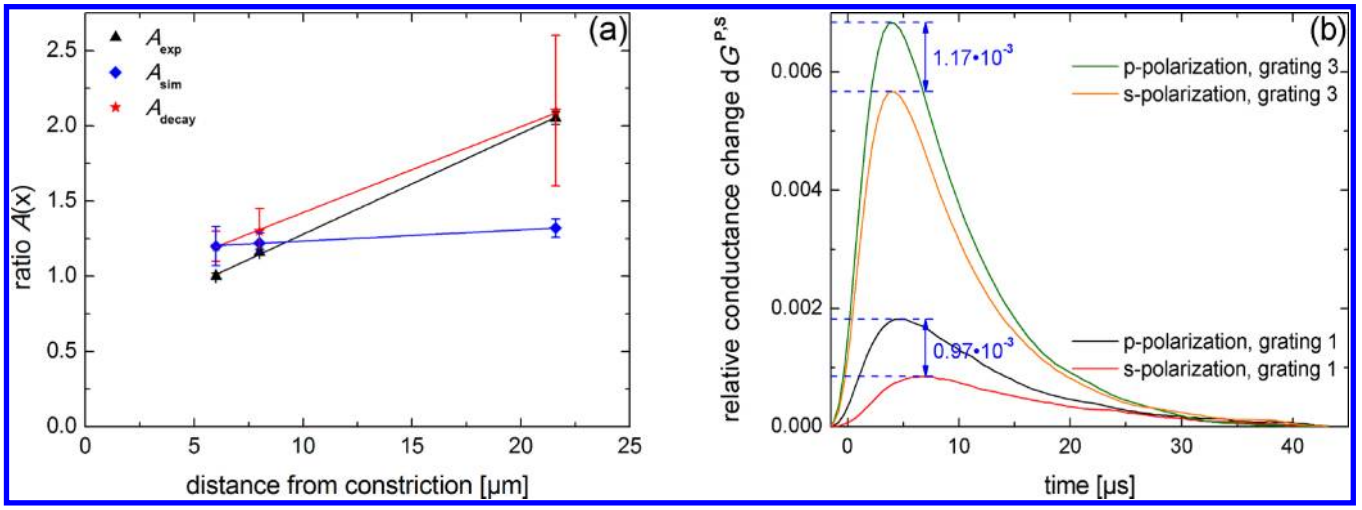

Figure 6. (a) Dependence of the ratio A on the distance from MPC to the position of illumination for the experimental (black triangles), simulation (blue diamonds), and decay length results (red stars). In the experiments, the ratio is increasing with the distance whereas the ratio is almost independent of the distance in the simulations (the straight lines serve as "guides to the eye"). The error bars for the simulations and for A_{exp} are obtained by averaging over data obtained for different heating powers. The error bars of A_{decay} refer to the uncertainties of the decay lengths l and $d_{therm,exp}$. (b) Time-resolved relative conductance change induced by a laser pulse when illuminating grating 1 or grating 3. The difference between the dashed blue lines indicates the influence of the $SPPs_{MPC}$ to the observed conductance enhancement. The conductance G of the sample remained constant at $(1.92 \pm 0.07)\ G_0$ throughout the whole measurement.

heat source we took into account the polarization-dependent excitation of SPPs at the gratings.

At first we study the time dependence of the thermal expansion after heating for both polarizations with the corresponding amount of heating power for a single laser pulse as in the experiments. Figure 4 shows the results obtained for different points of irradiation. The origin of the time axis t = 0 is at the maximum of the heating pulse (dashed line).

For both polarizations, the maximum thermal expansion (marked by the solid squares) is found at a delay time t_{sim} that increases with increasing distance, alike the observations for $dG^{P,S}{}_{max}$ in the experiments. A quantitative comparison between the delay times t_{exp} gained from experiments (triangles) and t_{sim} obtained from the simulations (squares) leads to Figure 5a. Overall the delay times in s-polarization exceed those in p-polarization, in the simulations as well as in the experiments. Furthermore, t_{exp} is slightly bigger than t_{sim} at all positions. The simulated delay time in s-polarization increases roughly with the square of the distance as expected for a diffusive transport mechanism, revealing that heat dissipation and phonon diffusion is the dominating mechanism. The difference between p- and s-polarization increases with the distance indicating that a faster transport process is contributing in p-polarization that we attribute to SPP transport. From a parabola fit $y = B_0 + B_1 x^2$ to the simulation results of the s-polarization case (red line), we deduce a heat diffusion constant D_{sim} of our system to $D_{sim} = 1/B_1 \approx (2.20 \pm 0.12) \times 10^{-4}$ m^2/s, in good agreement with the literature value $D_{Au,lit} = 4\kappa/(C_p\rho) \approx 2.80 \times 10^{-4}$ m^2/s (cf. ref 21) (κ_{Au} = 173 W/(m·K) is the reduced thermal conductivity due to the reduced film thickness,[22] C_p = 128 J/(kg·K) is the heat capacity at constant pressure, and $\rho = 19.3 \cdot 10^3$ kg/m^3 is the density of solid gold). This result shows that the heat

dx.doi.org/10.1021/nl502165y | Nano Lett. XXXX, XXX, XXX−XXX

transport in our system is dominated by the gold film and is directed in one dimension along the stripe, because of the high ratio between the heat conductivities of gold and polyimide (κ_{Au} = 173 W/(m·K), κ_{Poly} = 0.15 W/(m·K)) and despite the comparably small cross-section of the gold film (100 nm × 4 μm).

Another important conclusion can be drawn from Figure 4. The absolute length change of the thermal expansion is in the same range as in the time-dependent mechanical bending experiments by a piezo drive (see Figure S8b in the SI). Hence the thermal expansion is able to change the conductance considerably. Thus, the overall heating, i.e., heating by absorption of light and heating due to SPP decay, plays an important role for the conductance change, as already argued above. From the same data we obtain the thermal decay length by plotting the maximum expansion over distance and fitting an exponential decay function to it; see Figure 5b. The thermal decay length $d_{therm,sim}$ = (8.24 ± 0.17) μm is in very good agreement with the experimental value $d_{therm,exp}$ = (8.43 ± 0.02) μm deduced from the contribution to ΔG described in Figure 2.

In analogy to the experiments we study the development of the amplitude ratio A_{sim} between the polarizations as a function of distance (for details of the definition see the SI). At variance to the behavior of A_{exp}, A_{sim} is close to (1.26 ± 0.06) and independent of distance as would be expected for a purely thermal effect (see Figure 6a, blue diamonds).

Summarizing the simulation results, we find the same tendency as in the experiments regarding the delay time t. However, the simulations do not reproduce the experimental findings regarding the distance dependence of the amplitude ratio A. The additional effect has to be polarization-dependent and has to be longer ranged than d_{therm} because its effect enhances the conductance change when irradiating in p-polarization at very long distance from the MPC. We argue that this contribution is given by SPPs that arrive at the MPC and are even transmitted across the MPC with a relatively high probability in the order of 50%.[19] We denote these SPPs in the further text as $SPPs_{MPC}$. They may contribute to the conductance enhancement by PAT and by heating and thermal expansion, if they decay close to the MPC.

Comparing the simulation and experimental results, the described thermal effects decay on the scale of the thermal decay length $d_{therm} \approx 8.4$ μm. The conductance change in p-polarization contains contributions of the heating by absorption, of heating by SPP decay in the leads and of $SPPs_{MPC}$. The decay length of the SPPs is $l \approx 11.7$ μm.[19] As both characteristic quantities, d_{therm} and l are describing an exponential decay of a heat intensity $I_{0,heat}$ and of a SPP intensity $I_{0,SPP}$, we calculate the ratio $A_{decay}(x)$ between both as a function of the position of illumination analogously to the calculation of A_{exp}. This leads to

$$A_{decay}(x) = I_{SPP}(x)/I_{heat}(x) = [I_{0,SPP}\exp(-x/l)] / [I_{0,heat}\exp(-x/d_{therm,exp})] \sim \exp(-x/l) / \exp(-x/d_{therm,exp}) \quad (1)$$

whereby the initial values I_0 have to be determined, and l and $d_{therm,exp}$ are extracted from the simultaneous transport and optical measurements.[19] We obtain the distance dependence shown by the star-shaped, red symbols in Figure 6a.

The calculated ratios of A_{decay} show similar distance dependence as A_{exp}. Furthermore, the absolute values of these two ratios are in good agreement, implying that the initial values $I_{0,SPP}$ and $I_{0,heat}$ are of the same order, meaning that the contributions due to heat and $SPPs_{MPC}$ are in the same order of magnitude. For short distance the signal is dominated by thermal effects, while for longer distance $x \gg d_{therm}$ plasmonic effects become important. This is visualized in Figure 6b, where we plot the same data as in Figure 3, but without normalization. The observed conductance enhancements at the gratings consist of two contributions: The contribution induced by heating and the additional contribution in p-polarization. The second contribution has similar size $\approx 1 \cdot 10^{-3}$ for both positions. This identifies this second contribution to be the direct influence of $SPPs_{MPC}$ to the total conductance change dG, because the thermal expansion *difference* between the two polarizations should decrease with increasing distance (cf. Figure 5b), and the *ratio* between the two polarizations should be almost constant as Figure 6a (blue symbols) depicted. The relative contribution of the $SPPs_{MPC}$ to dG increases from roughly 1/6 (17%) at grating 3 to more than 50% at grating 1.

Whether these $SPPs_{MPC}$ contribute by the PAT mechanism or by thermal expansion to the conductance enhancement cannot be decided from the present investigations and remains subject of future experimental and simulation work. An estimation of their contribution calls for additional ingredients which require calculations and therefore will be published elsewhere.

Possible additional mechanisms, as e.g. the creation of a thermovoltage by the Seebeck effect can be ruled out, because we apply very low laser power and the signal remains unaffected upon inversion of the bias polarity. As the FE simulations showed the temperature enhancements at an area close to the MPC are in the range of 7 K when illuminating the gratings. According to ref 23, this would cause a thermovoltage in the range of 7 μV which is about 5 times smaller than the observed voltage drops across the MPC.

In conclusion, our studies of the optical and electronic responses of an atomic gold contact under irradiation with near-infrared laser pulses reveal the complexity of light-metal interaction at the nanoscale. By linking the optical and the transport results we elucidate the contribution of SPPs to the conductance change. We find a clear distance and polarization dependence of the conductance enhancement. Analyzing these dependences enables us to demonstrate the direct impact of SPPs to the conductance change by both, thermal expansion and PAT. The analysis of the transport experiments is additionally supported by FE simulations. Our findings are important for designing opto-nanoelectronic devices whose conductance is controllable by the excitation of surface plasmon polaritons.

■ ASSOCIATED CONTENT

Supporting Information

Additional information covering sample preparation, experimental setups, time-resolved electronic measurements, power-dependence of the light-induced conductance changes, accompanying optical measurements for both polarization states, and introduction of the time-resolved FE simulations. This material is available free of charge via the Internet at http://pubs.acs.org.

dx.doi.org/10.1021/nl502165y | Nano Lett. XXXX, XXX, XXX−XXX

AUTHOR INFORMATION

Corresponding Author

*E-mail: Elke.Scheer@uni-konstanz.de.

Present Address

P.N.: Department of Chemistry, University of Marburg, Hans-Meerwein-Straße, 35032 Marburg, Germany.

Author Contributions

D.B. fabricated the samples and performed the transport measurements. J.B. designed the optical setup. P.N. performed the optical measurements. R.W. designed the electronic setup. P.L. and E.S. initiated the project. All authors analyzed the data and discussed the results. The manuscript was written through contributions of all authors.

Notes

The authors declare no competing financial interest.

ACKNOWLEDGMENTS

We thank J. C. Cuevas, A. Erbe, S. Juodkazis, A. Leitenstorfer, M. Hagner, B. Kopp, M. Bädicker, J. C. Berres, A. Ganser, S. Dickreuter, G. Ghafoori, S. Nößner, T. Geldhauser, H. Misawa, and K. Ueno for valuable and fruitful discussions to this work. We gratefully acknowledge financial support from the Deutsche Forschungsgemeinschaft through SFB767 and the Strategic Japanese-German Cooperative Program of the JST and DFG on Nanoelectronics, from the Ministry of Science and Arts Baden-Württemberg through the Center of Applied Photonics, and the Baden-Württemberg-Stiftung in the framework of the Research Network Functional Nanostructures.

REFERENCES

(1) Agrait, N.; Yeyati, A. L.; van Ruitenbeek, J. M. *Phys. Rep.* **2003**, *377*, 81−271.

(2) Scheer, E.; Belzig, W.; Naveh, Y.; Devoret, M. H.; Esteve, D.; Urbina, C. *Phys. Rev. Lett.* **2001**, *86*, 284−287.

(3) Guhr, D. C.; Rettinger, D.; Boneberg, J.; Erbe, A.; Leiderer, P.; Scheer, E. *Phys. Rev. Lett.* **2007**, *99*, 086801.

(4) Guhr, D.; Rettinger, D.; Boneberg, J.; Erbe, A.; Leiderer, P.; Scheer, E. *J. Microsc.* **2008**, *229*, 407−414.

(5) Ittah, N.; Noy, G.; Yutsis, I.; Selzer, Y. *Nano Lett.* **2009**, *9*, 1615−1620.

(6) Ittah, N.; Selzer, Y. *Nano Lett.* **2011**, *11*, 529−534.

(7) Kolloch, A.; Benner, D.; Bädicker, M.; Waitz, R.; Geldhauser, T.; Boneberg, J.; Leiderer, P.; Scheer, E. *Proc. SPIE* **2011**, *8204*, 820404.

(8) Viljas, J. K.; Cuevas, J. C. *Phys. Rev. B* **2007**, *75*, 075406.

(9) Leiderer, P.; Bartels, C.; König-Birk, J.; Mosbacher, M.; Boneberg, J. *Appl. Phys. Lett.* **2004**, *85*, 5370−5372.

(10) Mühlschlegel, P.; Eisler, H.-J.; Martin, O. J. F.; Hecht, B.; Pohl, D. W. *Science* **2005**, *308*, 1607−1609.

(11) Merlein, J.; Kahl, M.; Zuschlag, A.; Sell, A.; Halm, A.; Boneberg, J.; Leiderer, P.; Leitenstorfer, A.; Bratschitsch, R. *Nat. Photonics* **2008**, *2*, 230−233.

(12) Boneberg, J.; König-Birk, J.; Münzer, H.-J.; Leiderer, P.; Shuford, K.; Schatz, G. *Appl. Phys. A: Mater. Sci. Process.* **2007**, *89*, 299−303.

(13) Farahani, J. N.; Pohl, D. W.; Eisler, H.-J.; Hecht, B. *Phys. Rev. Lett.* **2005**, *95*, 017402.

(14) Geldhauser, T.; Ikegaya, S.; Kolloch, A.; Murazawa, N.; Ueno, K.; Boneberg, J.; Leiderer, P.; Scheer, E.; Misawa, H. *Plasmonics* **2011**, *6*, 207−212.

(15) Prangsma, J. C.; Kern, J.; Knapp, A. G.; Grossmann, S.; Emmerling, M.; Kamp, M.; Hecht, B. *Nano Lett.* **2012**, *12*, 3915−3919.

(16) Ropers, C.; Neacsu, C. C.; Elsaesser, T.; Albrecht, M.; Raschke, M. B.; Lienau, C. *Nano Lett.* **2007**, *7*, 2784−2788.

(17) Ward, D. R.; Hüser, F.; Pauly, F.; Cuevas, J. C.; Natelson, D. *Nat. Nanotechnol.* **2010**, *5*, 732−736.

(18) Shi, S.-F.; Xiaodong, X.; Ralph, D. C.; McEuen, P. L. *Nano Lett.* **2011**, *11*, 1814−1818.

(19) Benner, D.; Boneberg, J.; Nürnberger, P.; Ghafoori, G.; Leiderer, P.; Scheer, E. *New J. Phys.* **2013**, *15*, 113014.

(20) Heeres, R. W.; Dorenbos, S. N.; Koene, B.; Solomon, G. S.; Kouwenhoven, L. P.; Zwiller, V. *Nano Lett.* **2009**, *10*, 661−664.

(21) Marin, E. *Lat. Am. J. Phys. Educ.* **2010**, *4*, 56−60.

(22) Langer, G.; Hartmann, J.; Reichling, M. *Rev. Sci. Instrum.* **1997**, *68*, 1510−1513.

(23) Ludoph, B.; van Ruitenbeek, J. M. *Phys. Rev. B* **1999**, *59*, 12290.